JOURNAL OF PROPULSION AND POWER
Vol. 19, No. 2, March–April 2003

Integration of an Aeroramp Injector/Plasma Igniter for Hydrocarbon Scramjets

L. S. Jacobsen,* S. D. Gallimore,† J. A. Schetz,‡ and W. F. O'Brien§
Virginia Polytechnic Institute and State University, Blacksburg, Virginia 24061-0203

A hydrocarbon-fuel injection and ignition/flame-holding system consisting of an aerodynamic-ramp injector and a DC plasma torch was designed for a scramjet vehicle operating from Mach 4 to Mach 8. It was tested in an unheated Mach 2.4 flow for initial evaluation. The injector consisted of two rows of two holes, angled downstream, and toed in to create additional vorticity and enhance mixing. The plasma torch was placed downstream of the injector at three different locations. The experiments involved ethylene injection through the aeroramp at jet-to-freestream momentum-flux ratios from 1.4 to 3.2. Methane and nitrogen were used as the main feedstocks for the plasma torch. The power output of the plasma torch varied from 1500 to 3000 W. Results showed that nitrogen outperformed methane, and increasing the oxygen content at the plasma/fuel-plume interface significantly improved the potential for ignition and flame propagation. The methane and nitrogen feedstocks performed best at the closest and middle downstream torch stations relative to the ethylene-fuel plume, respectively. Because of the low static freestream temperature (131 K), very little heat release was produced under these cold-flow conditions. Tests in a model scramjet combustor with hot flow are needed to complete the evaluation of this system. In addition, at all three torch stations, the counter-rotating vortex motion of the fuel-injector plume lifted up the plasma-torch plume. As a result, the downstream temperature-plume cores were 2.5 and 3.5 times higher at injector jet-to-freestream momentum-flux ratios of 1.5 and 3.0, respectively, compared to the torch alone.

Nomenclature

C_d	=	discharge coefficient
d_{eff}	=	effective diameter, $d_{\text{eq}}\sqrt{(C_d)}$
d_{eq}	=	equivalent jet diameter, $\sqrt{(4d_j)}$ for a four-hole array
d_j	=	jet diameter
h_{core}	=	height of the maximum total temperature-plume core
$h_{C_2,\max}$	=	maximum excited C_2 line penetration height
p	=	static pressure
$\bar{q}$	=	jet-to-freestream momentum-flux ratio
T_t	=	total temperature
u	=	flow speed
x	=	streamwise coordinate
y	=	spanwise coordinate
z	=	vertical coordinate
γ	=	specific heat ratio
ρ	=	density

Subscripts

j	=	injector
T	=	plasma-torch igniter
∞	=	freestream

Received 8 October 2001; revision received 3 December 2002; accepted for publication 14 December 2002.

*Graduate Research Assistant, Department of Aerospace and Ocean Engineering; currently NRC Research Associate, Aerospace Propulsion Office, Air Force Research Laboratories, Wright–Patterson Air Force Base, OH, 45433. Member AIAA.

†Graduate Research Assistant, Department of Mechanical Engineering; currently Aerospace Research Engineer, Hypersonic Airbreathing Propulsion Branch, Swales Aerospace, Langley, VA 23681. Member AIAA.

‡Fred D. Durham Chair, Department of Aerospace and Ocean Engineering. Fellow AIAA.

§Department Head, J. Bernard Jones Professor, Department of Mechanical Engineering. Associate Fellow AIAA.

Introduction

IN comparison to hydrogen, ignition and supersonic combustion with hydrocarbon fuels is a challenge. This is mainly because of the longer ignition delay and combustion times compared to hydrogen, which has been studied more extensively for use with scramjets in the past. Because of the difficulties associated with hydrocarbon fuels, both improved mixing and combustion enhancement are needed as compared to the existing scramjet combustor designs developed for hydrogen fuel.

In the pursuit of mixing enhancement, a multitude of experiments have been performed in the field of injection in supersonic flows using numerous techniques, such as swept ramps,[1–3] slots,[4,5] transverse injection,[1,6–11] and jet swirl.[12–17] An extensive review of injector mixing characteristics is given by Schetz et al.[18] The general interference effects generated by multihole transverse-injector arrays have been capitalized on, in the design of the aeroramp injector by Cox et al.,[19] Cox-Stouffer and Gruber,[20] Fuller et al.,[21] and Schetz et al.[22] This design shows promising features such as mixing characteristics near the same performance level of a physical ramp injector with lower pressure losses, while leaving a secondary core trapped in the shear layer near the wall. The effects of toe-in angle on a single-row injector array have also been examined by Jacobsen et al.[23] In that study, it was found that increasing the toe-in angle of the exterior injector holes greatly increased the mixing efficiency and core penetration of the overall jet plume generated by the array. Attempts to study the effects of an aeroramp injector array in a real scramjet combustor were first performed numerically by Eklund and Gruber[24] and then experimentally by Gruber et al.[25] In the latter study, two hydrocarbon-fueled aeroramps were compared to a single row of four 15-deg low-downstream-angled holes. A simplified four-hole aeroramp was also created by Jacobsen et al.[26] This aeroramp injector array showed improved mixing as compared to a single-hole low-downstream-angle injector. Jacobsen et al. also commented that the future development of the aeroramp should include the possibility of the incorporation of a flame-holding device somewhere in between or downstream of the fuel-injector array.

One favorable type of ignition aide and flame-holding device that has been used in supersonic combustion applications is the plasma torch. Over the years, several plasma torches have been developed involving continuous or pulsed operation.[27–30] Several experiments

have been performed pertaining to the use of a plasma torch as a main fuel igniter in crossflows.[30–41]

In this paper, we present an effort to combine the best features of the aeroramp injector and the plasma-torch igniter. Hence, we undertook to integrate and evaluate a new fuel injection and ignition/flame-holding system for use with gaseous hydrocarbon fuels in a scramjet combustor. The plasma torch was placed at three downstream locations relative to the fuel injector array. Initial evaluation of the device was performed in an unheated Mach 2.4 crossflow. Shadowgraph images and photographs of the combined ethylene-fuel and plasma-torch plume were taken at various momentum-flux ratios to help qualitatively understand the nature of the flows. Total temperature and emission spectra were also recorded at downstream locations to help quantify differences in the plasma-torches effectiveness as a potential igniter and flameholder.

Test Facilities

Experiments were performed in the Virginia Polytechnic Institute and State University 23 × 23 cm blowdown supersonic wind tunnel. The tunnel was configured with a convergent/divergent nozzle resulting in a freestream Mach number of 2.4. The test section dimensions were 23 cm wide by 23 cm high and 30 cm long in the streamwise direction. Data acquisition was performed with two personal computers and 16- and 32-channel 16-bit A/D converters. Figure 1 shows the wind-tunnel test section.

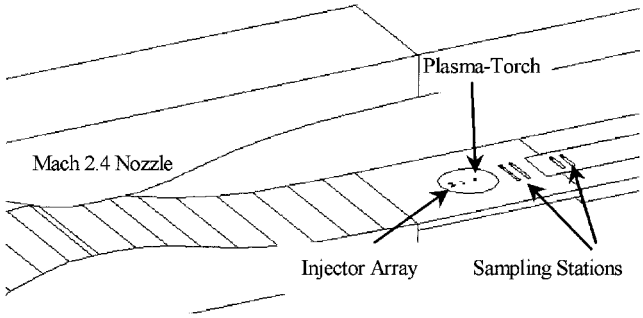

Fig. 1 Supersonic wind tunnel and test section.

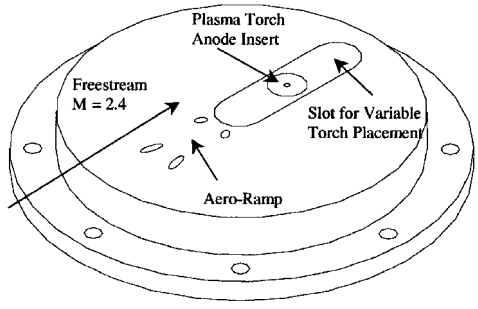

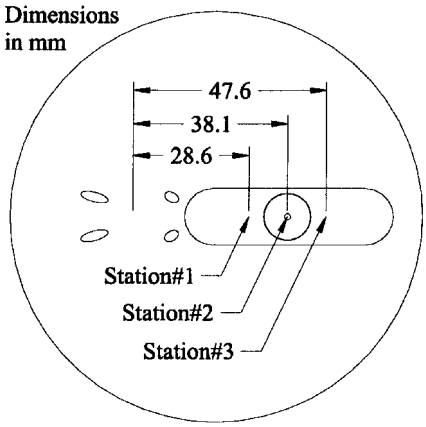

Fig. 2 Integrated aeroramp injector-array/plasma-torch igniter/flame holder.

Integrated Design

Figure 2 shows the injector model with an integrated plasma torch (the back hole) used in this study. The aeroramp injector had an equivalent jet diameter (diameter of the overall injector hole area) of 4.76 mm and consisted of two rows of two holes, spaced four equivalent jet diameters apart in the streamwise direction and with a cross-stream spacing of two equivalent jet diameters between the holes. The first and second pair of injector holes had transverse injection angles of 20 and 40 deg, respectively, with toe-in angles of 15 and 30 deg relative to the downstream axis. See Jacobsen et al.[26] for a complete description. For this study, the DC plasma torch was operated from about 1500 to 3000 W with various feedstocks. Different electrode materials were used depending on the torch feedstock. The integration of the aeroramp injector and plasma-torch igniter consisted of an aero-ramp, which was sized for planned combustion experiments (Jacobsen et al.[26]) and a plasma torch downstream of the centerline of the injector array. To vary the position of the torch relative to the array in this configuration, several slot inserts were created. The downstream torch location relative to the front of the injector array could be varied to 8, 10, or 12 d_{eq}.

Test Matrix

All wind-tunnel tests were performed at a freestream Mach number of 2.4. Experiments were performed first while injecting ambient air or ethylene fuel. The tunnel average freestream stagnation conditions were 3.7 atm and 281 K. These conditions resulted in a corresponding freestream velocity of 550 m/s and a unit Reynolds number of 4.2×10^7/m. Tests with air injection were run with jet-to-freestream momentum-flux ratios of 1.5–3.0. The jet-to-freestream momentum-flux ratio is defined as

$$\bar{q} = \frac{(\rho u^2)_j}{(\rho u^2)_\infty} = \frac{(\gamma p M^2)_j}{(\gamma p M^2)_\infty} \tag{1}$$

Ethylene from a supply tank was used as the injectant through the injector, block, and the momentum-flux ratios were limited to a maximum value of 3.5. A throttling valve in the line allowed reduction to a nominal value of 1.

The plasma torch was operated at a nominal jet-to-freestream momentum-flux ratio of 1.2 for all feedstocks used (methane, nitrogen, nitrogen plus hydrogen mixture 90/10 vol% and air). This momentum-flux ratio estimate was based on the plasma torch operational conditions neglecting the changes due to the heat addition from the arc.

The injector freestream flow coordinate system consists of right-hand Cartesian coordinates with the origin placed at the center of the injector array area. The positive x axis is in the downstream direction, the y axis in the horizontal direction, and the positive z axis in the vertical direction. The effective diameter was used to normalized axial distance. The effective diameter is defined as

$$d_{\text{eff}} = d_{\text{eq}}\sqrt{C_d} \tag{2}$$

where d_{eq} is the injector equivalent jet diameter. The injector discharge coefficient in the range studied for ethylene fuel was about 0.84. The equivalent jet diameter is defined as the diameter of an equivalent single jet that has the same total area of the four jets of the injector. The equivalent jet diameter for all four of the array jets was 4.76 mm. The plasma torch jet diameter, d_{torch}, was 1.59 mm.

Test Procedures

Shadowgraphs

Shadowgraphs were taken using a Hadland Photonics 4 charge-coupled device (CCD) Imacon 468 high-speed digital camera and a Spectra Physics 2.5 W continuous-beam argon-ion laser with a Model 265 exciter as the light source. To maximize power output from the laser, a broadband mirror was used to take advantage of all six wavelengths that the laser is capable of producing. This configuration made it possible to take pictures with exposure times of 2×10^{-8} s. The shadowgraph setup also consisted of the standard Z-formation optical mirrors, lenses, and a microscope lens for the laser. With a 20-ns exposure, it is possible to see the turbulent eddy structures in the flow significantly larger than 0.011 mm.

Plume Photography: Low-Speed Photographs

Pictures of the emission plumes produced in the combustion phase of the experiments were taken with a 35-mm camera and various bandpass filters, which enabled study of the excited-state species of the injectant-torch plumes.

Temperature Sampling

Temperature profiles were measured with a sampling rake consisting of three 1.59-mm-outer-diameter tubes spaced 6.4 mm apart, housing the thermocouples. Each tube had an inner diameter of 1.04 mm giving each probe a 0.85 mm^2 capture area. The total temperature probes each had four small holes drilled around the pipes to increase the recovery factors of the probes. Each total temperature probe's capture-to-recovery-area ratio was 5–1, which resulted in a recovery factor of 0.98. Exposed junction type-E thermocouples with 0.25-mm-diam beads were placed inside the three total temperature probes.

Emission Spectroscopy

Spectroscopic data was taken with an Ocean Optics S2000 3-CCD fiber-optic spectrometer. Each individual channel in the spectrometer had its own grating and CCD array with a spectral resolution of 0.08 nm. The overall spectral range observed by the three spectrometers was 196–730 nm. To localize the viewing area, a collimating lens was attached to the end of the fiber optic cable. This $f/2$ lens was made out of fused silica for use in the ultraviolet–visible infrared–near infrared. This reduced the width of the viewing area to about a 2.0 mm diam. Further reduction of the width of the viewing area to a 0.5 mm diameter was made with a scope that fit over the collimating lens. For more details on the spectrometer see Gallimore et al.[42]

Results and Analysis

Shadowgraphs

Shadowgraph images of the aerodynamic ramp injector and plasma torch in a Mach 2.4 flow are shown in Fig. 3. In all of the shadowgraph pictures the flow is from left to right. The boundary layer near the injector is about 1.9 d_{eq} thick. The bow shock waves produced from the two rows of injector holes in the injector array and the plasma torch turn downstream and to the right, approaching the angle of a Mach wave ($\approx$25 deg for $M = 2.4$). In these images, ethylene is being injected through the aeroramp injector at nominal jet-to-freestream momentum-flux ratios $\bar{q}$ of 1.5 and 3.0 and nitrogen is being injected through the plasma torch at a nominal $\bar{q}$ of 1.2 and a power level of 2000 W.

Figures 3a and 3b are shadowgraph pictures of the aeroramp and plasma torch by themselves. In Fig. 3a, details of the jet shock structure of the aeroramp can be seen, including the jet-plumes barrel shocks and the separation zone in front of the first pair of injectors. Evidence of a shock trail is also seen by a third highly oblique and somewhat unsteady shock, downstream of the aeroramp's first two injector-jet bow shock waves. Jacobsen et al.[26] have shown that the shock trail extends downstream with up to three oblique shock waves in this highly underexpanded flowfield. Because of the thickness of the boundary layer in relation to the plasma-torch jet in Fig. 3b, it is hard to detect any details pertaining to the plasma-jet shock structure in Fig. 3b. Note that, when operating at 2000 W, no illumination from the torch can be seen in the image. This was because of the high-intensity output of the laser light in comparison to the light produced by the torch in the direction of the optical setup in the 20-ns exposure time of the high-speed camera's CCD arrays.

The combined aeroramp and plasma-torch flowfield with the torch position at station 2 are presented in Figs. 3c and 3d. General trends include an increase in bow shock wave height and unsteadiness in the downstream bow shock of the aeroramp injector with increased jet-to-freestream momentum-flux ratio. Some condensation of ethylene in the area of the jet plumes is also shown, due to the sudden expansion of the highly underexpanded gas. This feature also increases with an increase of momentum-flux ratio. Another interesting feature of the integrated aeroramp/plasma-torch flowfield shown for the lower injector $\bar{q}$ conditions is the merging of the downstream recompression shock with the bow shock of the plasma torch. This feature is shown in both Figs. 3c and 3d. Note that in the farthest downstream torch position 3 the recompression shock is separated from the bow shock of the plasma torch. This is not apparent in the high injector $\bar{q}$ cases because the recompression shock is farther downstream. In all of the integrated configuration test cases, the plasma-torch bow shock is very unsteady with numerous kinks and emanating orthogonal shockwaves. This unsteadiness is indicative of increased turbulent mixing in this region. Weak orthogonal

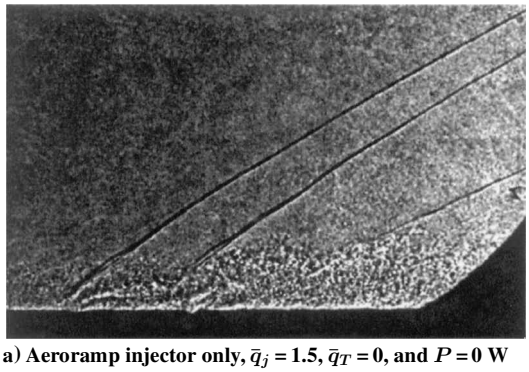

a) Aeroramp injector only, $\bar{q}_j = 1.5$, $\bar{q}_T = 0$, and $P = 0$ W

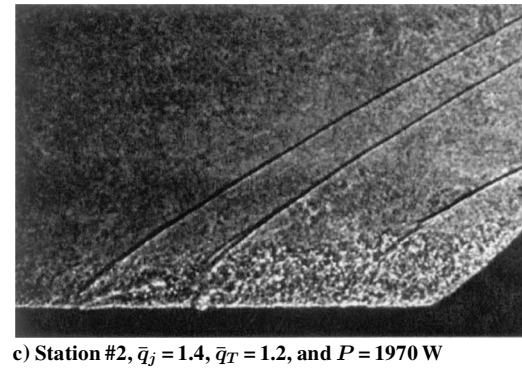

c) Station #2, $\bar{q}_j = 1.4$, $\bar{q}_T = 1.2$, and $P = 1970$ W

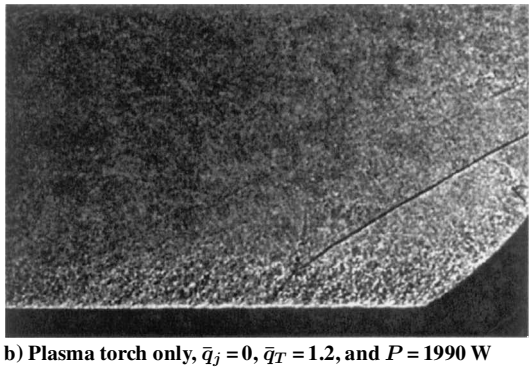

b) Plasma torch only, $\bar{q}_j = 0$, $\bar{q}_T = 1.2$, and $P = 1990$ W

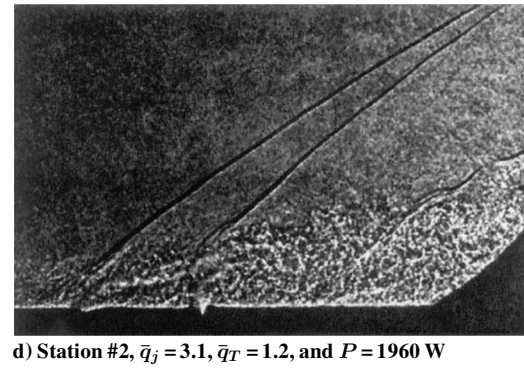

d) Station #2, $\bar{q}_j = 3.1$, $\bar{q}_T = 1.2$, and $P = 1960$ W

Fig. 3 Shadowgraphs of the integrated configuration and its components.

shock waves can also be seen emanating from the downstream bow shock of the aeroramp in the higher momentum-flux ratio cases.

Figures 3a and 3c shows two shadowgraph images taken nominally at the same injector and torch momentum-flux ratios. The difference between the two images is that one is taken with the torch not in operation and with no flow through it (Fig. 3a) and one is taken with the torch in operation at 1970 W (Fig. 3c). In the images, there is only a small difference in the position of the shock wave of the plasma torch injector relative to the recompression shock. Furthermore, this difference could be accounted for by image-to-image unsteadiness in the shock wave due to turbulence. Because no images were produced with the torch in operation at a higher power level, it is unclear how much the shock wave structure would change with additional energy input.

Figure 4 shows a set of sequential images taken with the 4-CCD Imacon 468 high-speed camera. The four images are spaced 6.06 μs apart, which allows the freestream to move 1 cm downstream during the sequence. This sequence was selected because in it an eddy structure of ethylene can be seen moving downstream just behind the shock wave. In addition, there is a local kink in the second injector row bow shock wave, which runs partially down its length as the clump moves farther downstream from the injector array. This is a good example of the way turbulent eddys in the jet/freestream mixing layer create unsteady motion in the bow shock structure by effectively creating additional intermittent blockage.

Time-Resolved Images

High-speed images of the chemiluminescence plumes generated by the integrated injector array/plasma torch were created with the Hadland Photonics Imacon 468 4-CCD digital camera. The high-speed images were taken 1.39 ms apart, with an integration time per frame of 10 μs. The images were spaced at one-quarter of the time it takes to go through one cycle of the rectified DC power supplies 180-Hz AC frequency (5.56 ms). Figure 5 presents the four images produced with a nitrogen torch feedstock at a nominal power level of 2000 W and ethylene fuel at a momentum-flux ratio of 1.5. The images are shown at twice their normal scale for closer inspection. In these images, the flow is from left to right and the emission plume generated from the plasma torch is seen emanating from the bottom left side of the images. Electrode fragments, emitted from the plasma torch, are the bright balls on the left-hand side of the

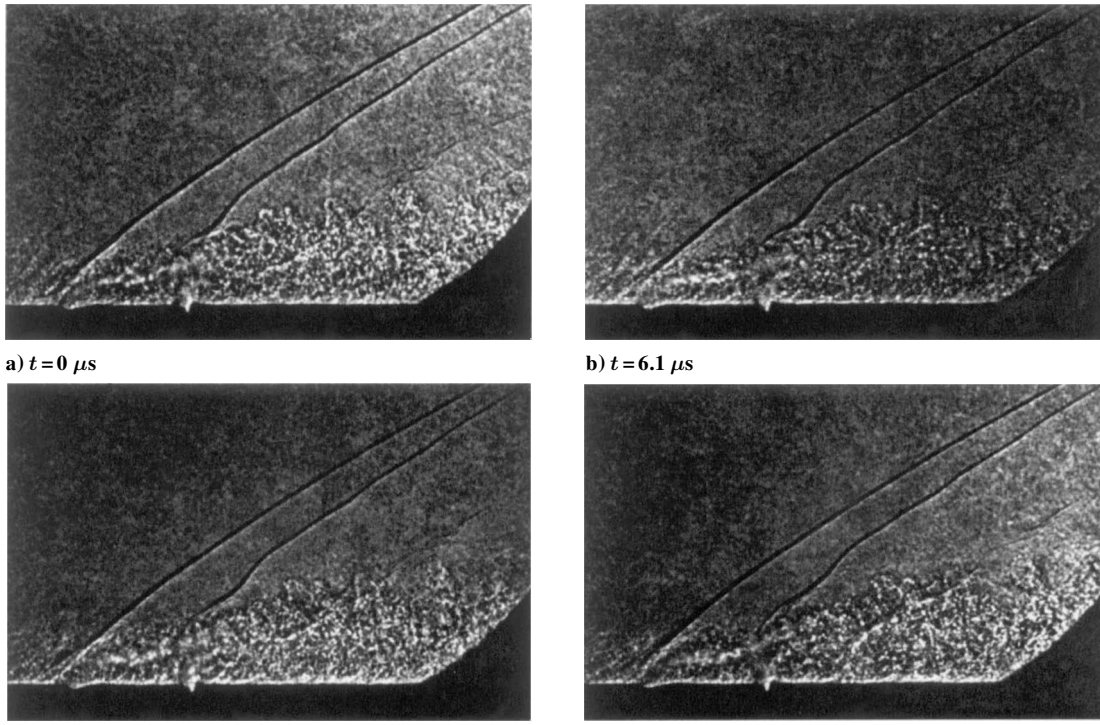

a) $t = 0$ μs **b)** $t = 6.1$ μs

c) $t = 12.1$ μs **d)** $t = 18.2$ μs

Fig. 4 High-speed sequential shadowgraph images; torch-station 1, $\bar{q}_j = 2.7$, $\bar{q}_T = 1.1$, and $P = 1990$ W.

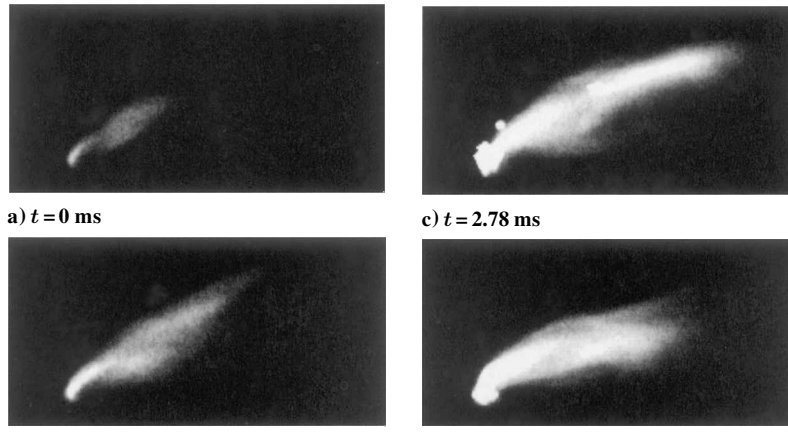

a) $t = 0$ ms **c)** $t = 2.78$ ms

b) $t = 1.39$ ms **d)** $t = 4.17$ ms

Fig. 5 High-speed flame plume images with nitrogen torch feedstock and ethylene fuel, $P = 2040$ W, $\bar{q}_j = 1.5$, $\bar{q}_T = 1.2$; 12.4 × 24.8 mm images.

plasma torch plume, near the orifice seen in Fig. 5c. The resulting emission is created from the interaction of the plasma torch plume with the ethylene fuel plume.

As is evident from the images, the emission plume size is very dependent on the cycle of the power supply. Note that the image in Fig. 5a is very dim for the camera integration time. This does not mean that the emission from the plume is necessarily as small as in the image, but rather that at that time in the power cycle the plume is emitting a lower level of intensity. This cyclic behavior may turn out to be very important, and further work should be done to attempt to vary the cyclic frequency. This, in turn, could lead to the excitation of possible resonant frequencies associated with the turbulence of the multiple-jet mixing processes.

A comparison of the scale of the plasma-torch emission plume to the injector-jet plume is shown in Fig. 6. In this image, the emission plume shown in Fig. 6 has been superimposed over a shadowgraph. To represent an averaged emission plume shape, the image is an overlay of all four images from Fig. 5. Both the emission plume and shadowgraph images are nominally at a power level of 2000 W, with nominal injector and plasma-torch momentum-flux ratios of 1.5 and 1.2. Both cases involve ethylene fuel and a nitrogen torch feedstock. As can be seen, the emission plume reaches about midway into the injector fuel plume. This shows that the emission plume is being lifted into an area with a lower overall equivalence ratio than that in the fuel cores, which could lead to entrainment into the upper portion of the jet/freestream mixing layer at the top of the fuel plume cores. If the potential flame reaches the top in a high-enthalpy flow, it would then have the chance to propagate through the mixing layer and spread around the entire fuel plume with help from the plume's vortex motion.

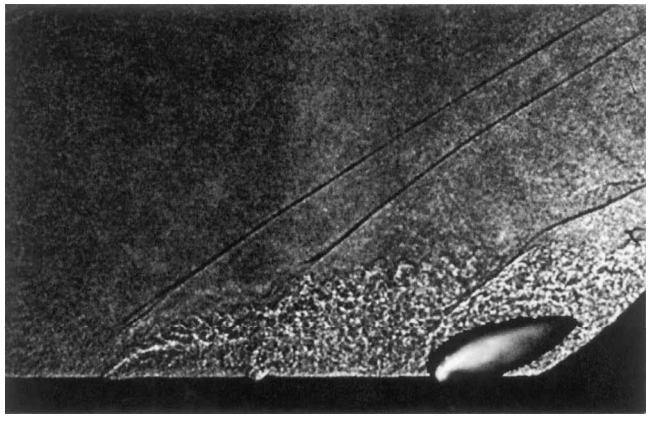

Fig. 6 Superimposed emission plume images embedded in shadowgraph image with nitrogen feedstock and ethylene fuel; shadowgraph: $P = 1970$ W, $\bar{q}_j = 1.4$, $\bar{q}_T = 1.2$, 60.7 × 94.2 mm image and emission plume image: $P = 2040$ W, $\bar{q}_j = 1.5$, and $\bar{q}_T = 1.2$.

Time-Averaged Phtotgraphs

Figures 7 and 8 show the low-speed (longer exposure time) emission plume photographs taken of the integrated configuration for nominal injector momentum-flux ratios of 1.5 and 3.0, with 1.2 for the plasma torch. These photographs were all taken with a 35-mm camera with a shutter speed of 1/250 s. They are unfiltered and the scale is 1:1, so that the actual sizes of the emission plumes are presented. In all of these photographs, the flow is from left to right, and the plasma torch is situated behind the aeroramp fuel-injector array at station 1, 2, or 3, excluding the plasma-torch plume pictures in Fig. 8. The smaller plume images to the right in some of the photographs are reflections off the fused silica glass on the other side of the test section. In all the photographs, the emission plumes are eventually quenched before further propagation into the main flow can be achieved. This is primarily due to the very low static freestream temperature (131 K) of the wind-tunnel facility. With this in mind, one can speculate that whichever ethylene-fuel/plasma-torch feedstock combination produces the largest emission plume in this cold, harsh environment would probably lead to the highest level of main flow/fuel ignition, combustion, and flame propagation in a higher enthalpy environment where supersonic combustion applications are used.

A comparison between methane and nitrogen torch feedstocks is given in Fig. 7 with a nominal torch power of 2000 W at a nominal

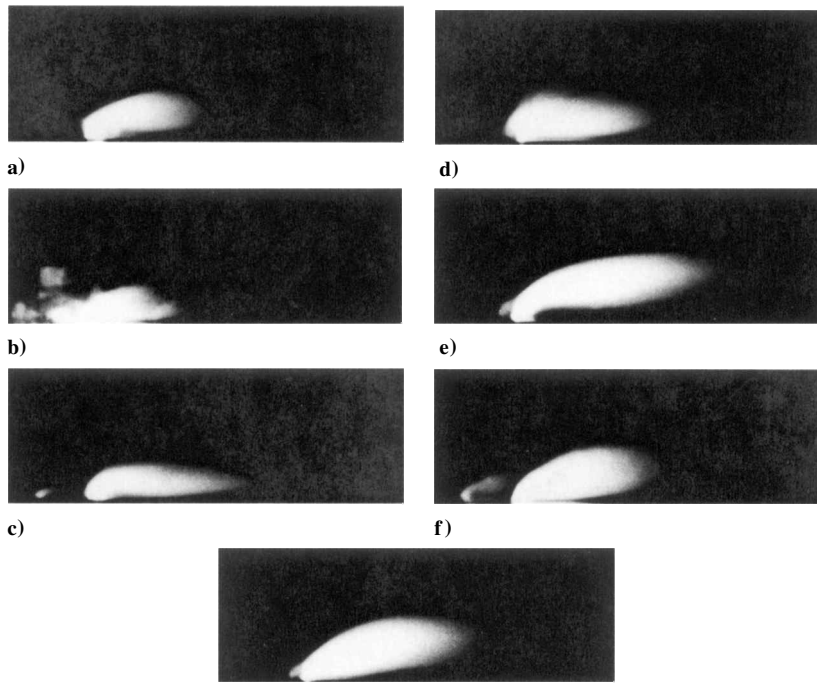

Fig. 7 Emission plume photographs of integrated configuration with ethylene-fueled injector and CH_4, N_2, or $N_2 + H_2$ torch feedstocks; 17.8 × 52.3 mm images: a) Station #1, methane feedstock, $\bar{q}_j = 1.6$, $\bar{q}_T = 1.2$, and $P = 2070$ W, b) Station #2, methane feedstock, $\bar{q}_j = 1.4$, $\bar{q}_T = 1.1$, and $P = 1990$ W, c) Station #3, methane feedstock, $\bar{q}_j = 1.5$, $\bar{q}_T = 1.3$, and $P = 2070$ W, d) Station #1, nitrogen feedstock, $\bar{q}_j = 1.5$, $\bar{q}_T = 1.2$, and $P = 1970$ W, e) Station #2, nitrogen feedstock, $\bar{q}_j = 1.5$, $\bar{q}_T = 1.2$, and $P = 2020$ W, f) Station #3, nitrogen feedstock, $\bar{q}_j = 1.5$, $\bar{q}_T = 1.2$, and $P = 2050$ W, and g) Station #2, $N_2 + H_2$ feedstock, $\bar{q}_j = 1.5$, $\bar{q}_T = 1.2$, and $P = 2090$ W.

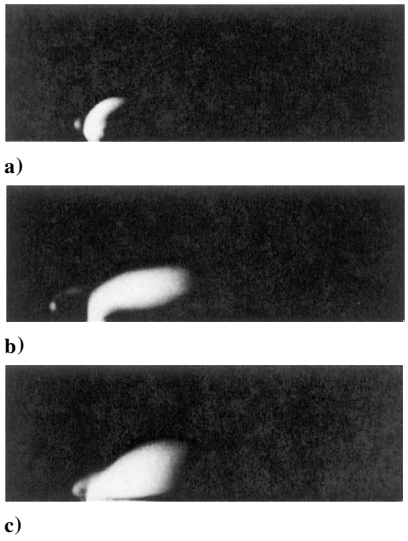

Fig. 8 Emission plume photographs of plasma torch with a nitrogen feedstock at different injector jet-to-freestream momentum-flux ratios; 17.8 × 52.3 mm images: a) Nitrogen feedstock, $\bar{q}_j = 0$, $\bar{q}_T = 1.3$, and $P = 1520$ W, b) Station #2, nitrogen feedstock, $\bar{q}_j = 1.6$, $\bar{q}_T = 1.3$, and $P = 1570$ W, and c) Station #2, nitrogen feedstock, $\bar{q}_j = 2.9$, $\bar{q}_T = 1.2$, and $P = 1520$ W.

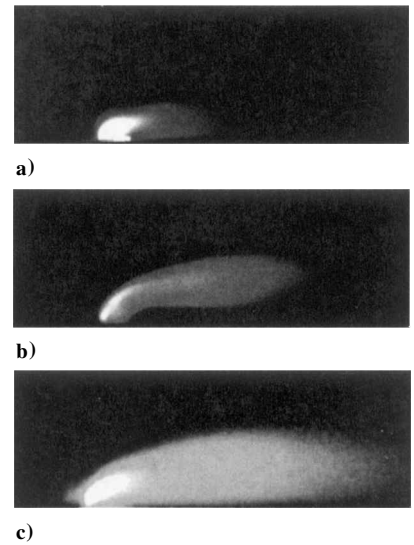

Fig. 9 Filtered emission plume photographs, 390-nm bandpass filter, FWHM ± 10 nm, power nominally 3000 W; 17.8 × 52.3 mm images: a) Station #2, methane feedstock, $\bar{q}_j = 1.5$, and $\bar{q}_T = 1.2$, b) Station #2, nitrogen feedstock, $\bar{q}_j = 1.5$, and $\bar{q}_T = 1.2$, and c) Station #2, air feedstock, $\bar{q}_j = 1.5$, and $\bar{q}_T = 1.2$.

aeroramp momentum-flux ratio of 1.5. A bright white portion was seen with a light blue color on the outer edge of the downstream portion of the emission, which is common with the combustion of ethylene and air. The bright white portion of the emission is a highly excited region. In the methane torch feedstock photographs (Figs. 7a–7c), the emission plume penetrates the farthest with the torch at station 1, but it appears to have the longest plume with the torch at station 3. The nitrogen feedstock emission plumes (Figs. 7d–7f) are larger than the methane plumes, and the torch-station 2 photographs shown in Fig. 7e has the largest plume with the highest penetration level.

Figure 8 shows the photographs of the plasma torch in a Mach 2.4 crossflow by itself with no fuel from the injector and with the injector in operation at nominal injector momentum flux ratios of 1.5 and 3.0. In all three images of Fig. 8, nitrogen was used as the torch feedstock at a power level of 1500 W. In all of the photographs, the nominal plasma-torch jet-to-freestream momentum-flux ratio was 1.2. Figure 8 was created to emphasize the lifting effect of the plasma torch plume by the aeroramp fuel array and the additional luminescence created by the interactions of the nitrogen plasma with the fuel jet. On the effect of lifting, it appears that the initial shape of the plasma jet itself, as shown in Fig. 8a, is very similar in shape to the lower momentum-flux ratio image shown in Fig. 8b ($\bar{q} = 1.5$), but without the additional luminescence plume downstream. However, as the momentum-flux ratio is increased to 3.0, as shown in Fig. 8c, the top portion of the luminescence plume is raised and much broader in the vertical direction. This is thought to be due to the additional size of the aeroramp fuel plume as the injector is operated at a higher equivalence ratio. Furthermore, because the plasma jet is actually inserted between the two rows of streamwise jets, the increase in vertical breadth could be thought of as cross-stream contraction of the plasma core from the additional momentum of the fuel plume.

Also note that the chemiluminescence (emission) plume reaction zone is not necessarily the path of the plasma-jet feedstock. This was made evident by inspecting the differences in shape of the emission from the operation of the torch with the methane and nitrogen feedstocks behind the fuel-injector array. For example, at torch-station 2, the methane feedstock produced the highest amount of emission near the surface, whereas the nitrogen feedstock emission plume was more prone to penetrate up off of the surface of the test section. Without a significant pressure rise in the vicinity of the plasma jet, the path of the two feestocks should be more or less similar. Hence, the emission seen is really the path of the reaction as altered by the local change in equivalence ratio due to the plasma-torch feedstock.

The general trend of the increase in power for torch-station 2 with the torch in operation with a nitrogen feedstock can be seen by comparison of Figs. 8b (1500 W) and 7e (2000 W). In both Figs. 8b and 7e, the fuel injector and torch are operated at nominal jet-to-freestream momentum-flux ratios of 1.5 and 1.2, respectively. From the photographs, it is seen that as the power is increased by about 33% the downstream plume length has almost doubled. The significance of this growth in downstream plume length is that it indicates that some heat release must be taking place in the chemiluminescence plume. This indicates that there may be a point where the reaction becomes self-sustaining as the power level is increased, that is, not quenched.

Figure 9 shows some of the low-speed photographs taken of the plasma torch in operation at 3000 W behind the aeroramp injector ($\bar{q} = 1.5$) at station 2 with methane (Fig. 9a), nitrogen (Fig. 9b), and air (Fig. 9c) as the torch feedstocks. The photographs were taken through a 390-nm bandpass filter [full width at half-maximum (FWHM) = ±10 nm] with an exposure time of 1/30 s, which for the chemiluminescent plumes lets in light from the CH/CN/N_2 lines. Thus, the photographs are a good marker for the plasma zone of the torch chemiluminescence plume. From the three photographs, it is evident that the emission plume produced with air is larger than the one produced by nitrogen, which is in turn larger than the one with the methane feedstock. The photograph shown in Fig. 9c with air as the torch feedstock is from a preliminary set of data and was added to show the potential of air as a feedstock. With the air feedstock producing a larger plume than the nitrogen and, in turn, methane feedstock, one must ask if the ignition process in this region is mixing dominated. Because as the reaction region is less deprived of oxygen, the flame increases in size. Further evidence of this conclusion is shown in Fig. 7g, with the torch in operation with the nitrogen hydrogen mixture at torch-station 2, because the flame is noticeably smaller than the nitrogen plume alone and is approaching the general shape of the methane feedstock configuration at torch-station 2, shown in Fig. 7b. This would also open up the possibility that the configuration may work better with the torch in operation farther downstream of the fuel injector array. The only downside to this is that farther downstream, the plasma jet may not be able to take advantage of the lifting effect of the fuel jet and may only ignite the portion in between, and not mix or propagate around, the aeroramps two fuel-plumes cores. With this general oxygen-starved mixing relationship in mind, one must conclude that when attempting to ignite

a hydrocarbon-fuel jet with a plasma torch downstream of the jet, pure oxygen plasma must work best. This also implies that the reduction in ignition delay from the production of thermal NO through the Zeldovich mechanism is a second-order effect when compared to general effects of mixing on combustion in the hydrocarbon fuel jet in a supersonic crossflow. A mixing-dominated-type flowfield must also imply that the integrated configuration, for a given torch station, would have greater success at main fuel ignition the lower the injector momentum flux ratio goes. Because, in general, as the momentum-flux ratio is decreased, the local equivalence ratio of the fuel plume at the torch location lowers as the jet becomes leaner.

Total Temperature Profiles

Figures 10 present the results from the total temperature surveys made downstream of the integrated injector array and plasma torch. Total temperature data was taken at stations 1, 2, and 3 with methane, nitrogen, and a mixture of nitrogen and hydrogen (90/10 vol%) as the torch feedstocks with a $\bar{q}$ of 1.2 ± 0.1 and an injector $\bar{q}$ of 1.5 ± 0.1 and 3.0 ± 0.15 with ethylene injection. The results from the integrated configuration with methane and nitrogen feedstocks at a power level of 2000 W and with the fuel injector at a $\bar{q}$ of 1.5 ± 0.1 are presented here. All of the total temperature profiles were made with the torch in operation at 1500 or 2000 ± 75 W. These cross-stream, isotherm profiles consist of measurements taken just over $x/d_{\text{eff}} = 29$ downstream from the center of the overall area of the aeroramp injector holes. The three torch stations were 6.5, 8.7, and 10.9 x/d_{eff}, respectively, downstream from the center of the overall injector area. This also corresponds to downstream distances from the center of the plasma-torch hole to the temperature sampling plane of 62.4, 56.4, and 50.4 x/d_{torch}.

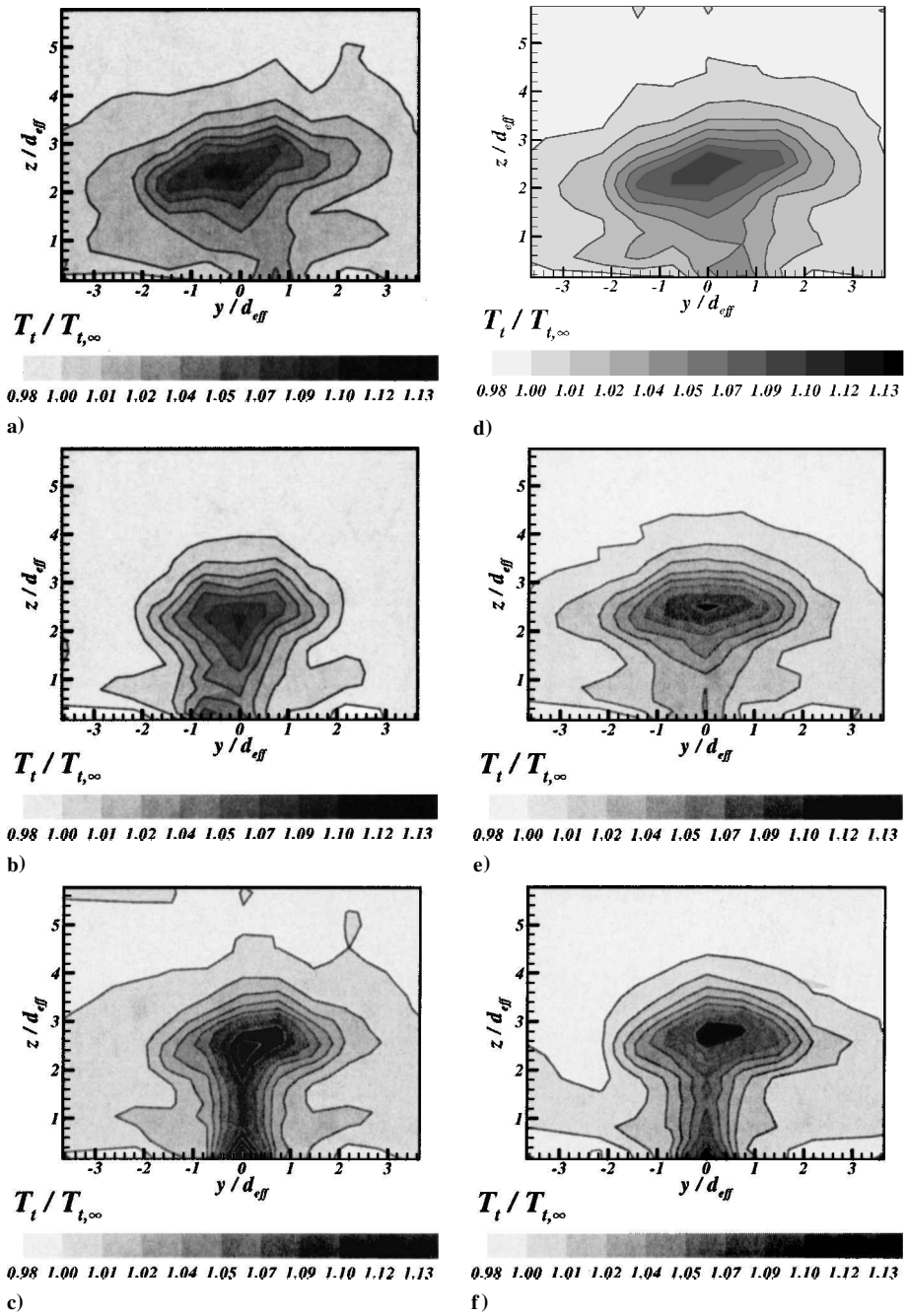

Fig. 10 Downstream total temperature plumes showing variation of torch station with methane and nitrogen feedstocks, power nominally 2000 W: a) Torch-station #1 methane feedstock, $\bar{q}_j = 1.5$, and $\bar{q}_T = 1.2$, b) Torch-station #2 methane feedstock, $\bar{q}_j = 1.5$, and $\bar{q}_T = 1.2$, c) Torch-station #3 methane feedstock, $\bar{q}_j = 1.5$, and $\bar{q}_T = 1.2$, d) Torch-station #1 nitrogen feedstock, $\bar{q}_j = 1.5$, and $\bar{q}_T = 1.2$, e) Torch-station #2 nitrogen feedstock, $\bar{q}_j = 1.5$, and $\bar{q}_T = 1.2$, and f) Torch-station #3 nitrogen feedstock, $\bar{q}_j = 1.5$, and $\bar{q}_T = 1.2$.

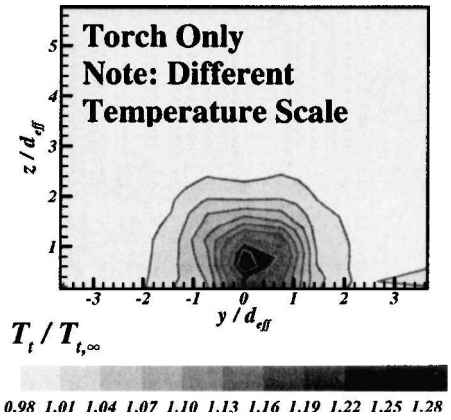

a) Torch-station #2, $\bar{q}_j = 0.0$, and $\bar{q}_T = 1.2$

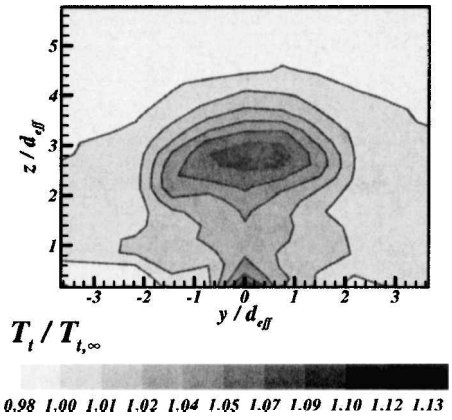

b) Torch-station #2, $\bar{q}_j = 1.5$, and $\bar{q}_T = 1.2$

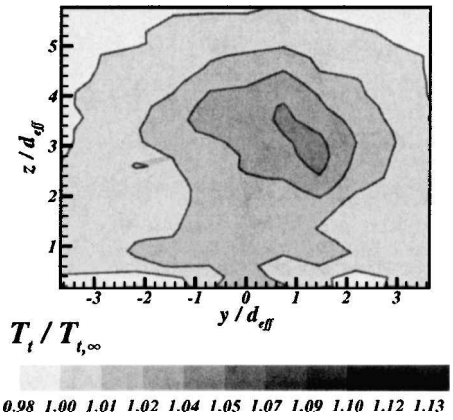

c) Torch-station #2, $\bar{q}_j = 3.0$, and $\bar{q}_T = 1.2$

Fig. 11 Downstream total temperature plumes showing effects of the injector jet-to-freestream momentum-flux ratio with a nitrogen feedstock, power nominally 1500 W.

The results for the torch in operation at 1500 W at torch-station 2 without the fuel injector and at nominal jet-to-freestream momentum-flux ratios of 1.5 and 3.0 are presented in Fig. 11. The scale of the total temperature profiles with the plasma torch in operation by itself (Fig. 11a) was set to a different scale from that of Figs. 11b and 11c, because the torch cores alone were much hotter since they did not have a large counter-rotating vortex pair to disperse the torch jet. In addition, Figs. 11b and 11c are also set to the same scale as the temperature profiles in Fig. 10. The general lifting effect of the torch plume and its entrainment into the fuel plume is shown by comparing the torch alone in Fig. 11a to the integrated configuration shown in Figs. 11b and 11c. As the momentum-flux ratio of the fuel injector is increased, the torch core plume temperature drops, and the plume height, width, and overall area are greatly increased.

Some of the general trends associated with the temperature profiles of the plasma torch using a nitrogen feedstock and ethylene fuel from the injector involved the widening of the temperature plume as the torch is moved farther upstream. This effect was due to an increase in distance between the torch and the total temperature probe, which allows the torch plume to mix further with that of the injector and the mainstream. This trend was not fully observed in the profiles with methane as the torch feedstock (Fig. 10a). In the methane feedstock cases, the plume is still the largest with the torch at the near station, it continues to shrink as the torch is moved from torch-station 1 to torch-station 2, but then grows slightly again from torch-station 2 to torch-station 3. This trend is also observed in methane feedstock emission plume photographs shown in Fig. 7.

In the profiles with the torch in operation at torch-station 3 for both methane and nitrogen feedstocks (Figs. 10c and 10f), there is a secondary temperature core near the surface of the test section floor. This implies that the plasma torch station is far enough downstream that its plume does not get entirely entrained into the fuel injector plume. In these two profiles, the main temperature plume cores are shown to be off-center to the right side in the positive y direction. This off-center behavior is also apparent in the nitrogen plasma torch profile, with the torch in operation alone, shown in Fig. 11a. This general effect could be due to the width between sampling stations, or to some relationship between the swirling of the torch plume and its effects on the mixing layer. Note that there was a flow swirler inside the plasma torch, which had a swirl number of 1.0. The swirl number is defined here as the ratio of tangential to streamwise velocity of the jet at the exit plane of the flow swirler. That direction of swirl corresponds to a counterclockwise rotation on the profiles, which is interesting because the plasma plumes temperature is off-center in the other direction (right) near the core. This may mean that there could be a relationship between the counter-rotation effects of the torch and injector plumes and the asymmetric mixing of the temperature field. From the temperature profiles for the torch at the closer station relative to the injector fuel plume (Figs. 10a and 10d), it is apparent that the temperature plume core is now off-center toward the left. Furthermore, the temperature profiles with the torch at station 2 shown in Figs. 10b and 10e appear to be symmetric. Therefore, as the torch is moved farther away from the fuel injector array, the total temperature plume core is shifted from left to right. Whether this would influence ignition and combustion of the main plume in a high-enthalpy environment is not known. However, symmetric burning of both sides of the fuel plume would definitely be desirable. This effect was also seen in the high-momentum-flux ratio (3.0) profiles, but in those profiles, the temperature plumes were all, to some degree, shifted slightly over to the right-hand side of the injector fuel plume, although the same left to right trend of the first through third torch stations was preserved. This is probably due to additional vortex strength from the higher momentum-flux ratio levels.

Another interesting feature of the plumes in Fig. 10 is that the core temperature with the torch at torch-station 1 is very comparable to that at station 2. This may indicate a higher level of heat release due to the reactions in the plasma/plume interface because having the plume at a location farther upstream should tend to mix the temperature to a lower level by the time it gets to the temperature probe sampling location. This seems to be counter to the visible size of the plumes as shown in Fig. 7. However, one must remember that the visible size of the plume as seen from the side view of a wind tunnel does not necessarily give us any indication to its width or the extent of heat release inside its region past the general output in luminosity produced by the plume.

Total Temperature Plume Core Trends

Figures 12 and 13 are graphs of the plume core temperature and penetration height, respectively, which were created from the total temperature surveys. In Figs. 12 and 13 data are presented for the aeroramp operating at a $\bar{q}$ of 1.5 with the torch at a $\bar{q}$ of 1.2 and the torch in operation alone. In both cases, the torch is operating at 2000 W with methane, nitrogen, and nitrogen/hydrogen mixture

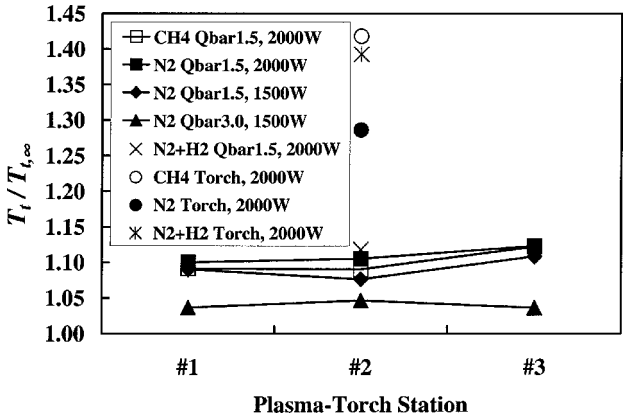

Fig. 12 Downstream total temperature plume core maximum temperatures.

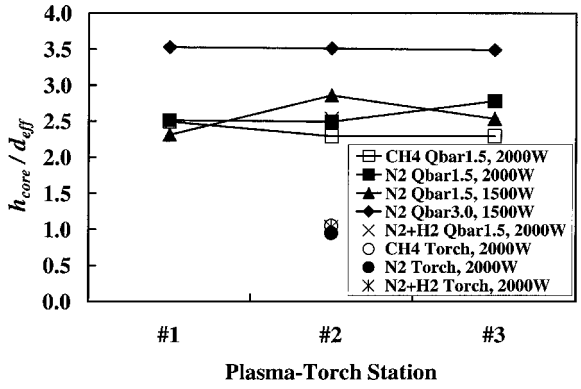

Fig. 13 Downstream total temperature plume core maximum penetration height.

feedstocks. There is also data presented for the injector operating at a $\bar{q}$ of 1.5 and 3.0 with the plasma torch operating with a nitrogen feedstock at 1500 W at a $\bar{q}$ of 1.2. These results show that the plumes generated with the nitrogen torch feedstock and ethylene fuel were, in general, hotter and penetrated farther than those produced with the methane feedstock. The penetration trends also affect the increase of $\bar{q}$ on the overall height of the temperature plume core. The general penetration height of the plume core is roughly 2.5 and 3.5 times higher with the torch in operation with fuel injector $\bar{q}$ of 1.5 and 3.0, respectively, as compared to operation alone.

Emission Spectroscopy

Spectroscopic measurements were performed while injecting ethylene through the aeroramp injector and methane, nitrogen, nitrogen/hydrogen mixture, or air feedstocks through the plasma torch igniter. Data were measured for the aeroramp injector at nominal momentum-flux ratios of 1.5 and 3.0 with the plasma torch at stations 1, 2, and 3 and a nominal torch momentum flux ratio of 1.2.

General spectrograms for the main feedstock/injector combinations are presented in Figs. 14–16. The intensity scales in these graphs are equal for ease to aid in interpretation of the magnitudes between various feedstocks, and all of the data were collected with an integration time of 0.125 s. Results are shown for the nitrogen and methane plasma-torch feedstocks at their corresponding "brightest" torch station and vertical height. The results in Figs. 14–16 were created with the three-channel fiber optic spectrometer.

Figure 14 shows the spectral line data for the 200–400 nm range with the plasma torch operating at 2000 W with a nitrogen feedstock downstream of the ethylene-fuel injector. Definite peaks were identified for monotonic carbon C* (247.9 nm), and the CN(0, 0) band (388.3 nm). The CN* band is part of a strong violet system which

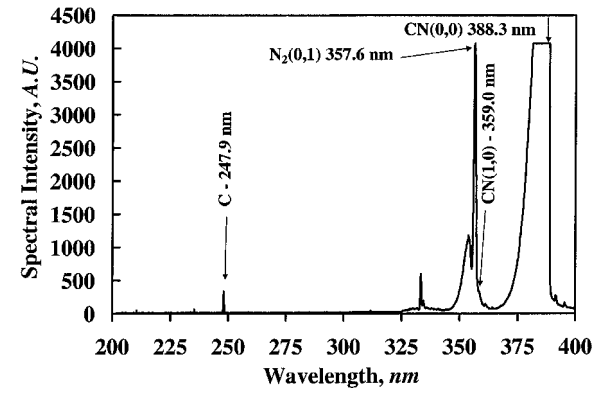

Fig. 14 Typical spectrogram, nitrogen feedstock, ethylene fuel, 200–400 nm range.

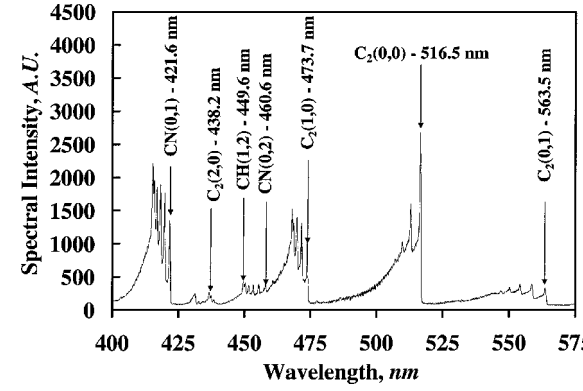

Fig. 15 Typical spectrogram, nitrogen, feedstock, ethylene fuel, 400–575 nm range.

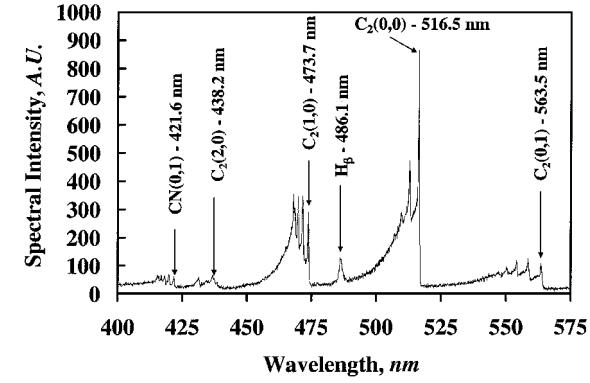

Fig. 16 Typical spectrogram, methane feedstock, ethylene fuel, 400–575 nm range.

appears in arc sources containing, of course, nitrogen and carbon compounds, and has heads at 359.0 (1, 0), 388.3 (0, 0), 421.6 (0, 1), and 460.6 nm (0, 2) degraded to the violet.[43] Other more questionable peaks in Fig. 14 are shown at 333.4 and 356.5 nm. These peaks are more questionable because there are a lot of peaks (CN*, NH*, N_2^*, CN*) at and around the 333–334 nm range and the peak shown as N_2^* at 357.6 nm is actually on the graph as 356.7 nm. This 1-nm discrepancy in wavelength could be due to many factors, ranging from miscalibration of the spectrometer or Doppler shifting of the line due to the high flow velocity. Furthermore, this area has multiple possibilities for peaks and definite superposition of the local CN(1, 0) band onto the rest of the area. In addition, the N_2^* band in regular flames usually has a secondary peak (2, 1) at 353.7, which has been shown to have an intensity of about 80% of the (1, 0) peak.[43] Thus, there must be some significant contribution to the apparent (1, 0) peak from some other excited species.

Figure 15 shows the spectral data for the 400–575 nm range with the nitrogen feedstock and ethylene fuel at 2000 W. The peaks shown in this spectrogram are more readily identifiable than those in the 200–400 nm range. First, the CN* 421.6- (0, 1) and 460.6-nm (0, 2) bands, degraded to the violet, are shown. The most prevalent system shown in this spectral range is the C_2^* Swan bands, with its most prevalent bands ranging as follows: 438.2 (2, 0), 473.7 (1, 0), 516.6 (0, 0), 563.5 (0, 1), and 619.1 nm (0, 2). Typically, these bands degrade to the violet and are very common in sources containing carbon, such as Bunsen flames and in discharges through hydrocarbons and other organics.[43] They also appear in a carbon arc and in active nitrogen reacting with organic vapors. A small bandlike structure is also apparent at 431.5 nm, which degrades to the violet. Another small additional peak is evident at the tail end of the CN (0, 2) band and is located around 449.7 nm. This could be part of the 390.0-nm CH* system because there is another band (1, 2) from this system at 449.5 nm. However, because the 388.9-nm peak would be washed out from the CN (0, 0) band, it is hard to say with utmost certainty that this is CH*. Note that the overall intensity of the apparent CH* band is fairly low as compared to the major chemiluminescence of the plume.

Spectral data for the 575–750 nm range with the nitrogen and methane feedstocks and ethylene fuel at 2000 W were also collected. The only major line in this range for both configurations was the monatomic H_α line at 656.3 nm and, thus, no figure is presented. The H_β line is shown in Fig. 16. Figure 16 shows spectral data in the 400–575 nm range with methane as the torch feedstock in operation at 2000 W and ethylene fuel. The H_β line is at 486.1 nm and is more apparent in the methane spectral data because methane plasma involves the direct dissociation and excitation of hydrogen instead of by indirect means of the ethylene stream, as with the nitrogen plasma. For the other peaks presented in this region, the only real difference between the methane and nitrogen feedstock spectra is the decrease in the relative intensity of the CN* bands, which were the dominant bands, intensity wise, in the nitrogen spectra.

The main intensity trends of the spectral line data obtained while using nitrogen and methane feedstocks as a function of torch station relative to the injector array are presented in Figs. 17 and 18. These data points represent the maximum intensity locations of a vertical sweep with the spectrometer placed 1.0 cm downstream from the exit of the torch. During these experiments, the spectrometer had a 0.125-s integration time at each station with a local viewing area with a diameter of 0.5 mm. Because of the location of the fused silica windows relative to the plasma torch, it was necessary to place the spectrometer at a 3-deg angle off the perpendicular to make measurements at torch-station 3. The results show that the torch stations with the brightest spectral line intensities were stations 2 and 1 for nitrogen and methane, respectively. In addition, they show that the spectral line intensities all share the same general trends of variation in intensity as a function of torch location relative to the fuel-injector array for the two main feedstocks tested.

More results for the data obtained while using methane and nitrogen feedstocks are presented in Figs. 19 and 20. Figures 19 and

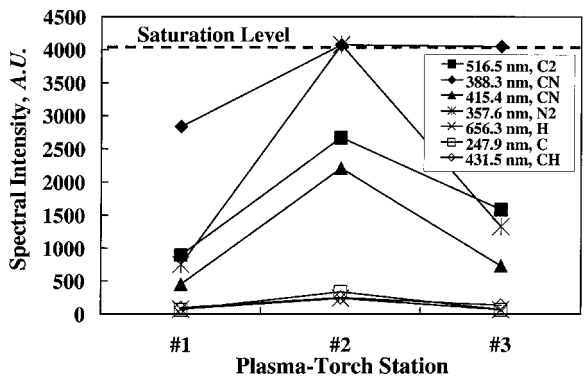

Fig. 17 Spectral line intensity trends as a function of plasma-torch station, nitrogen feedstock, ethylene fuel, 2000 W, $\bar{q}_j = 1.5$ and $\bar{q}_T = 1.2$.

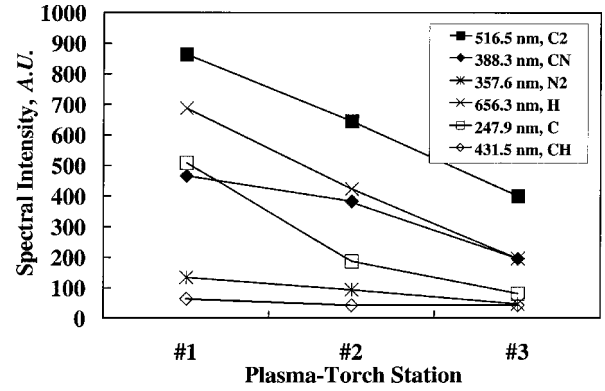

Fig. 18 Spectral line intensity trends as a function of plasma-torch station for methane feedstock and ethylene fuel, 2000 W, $\bar{q}_j = 1.5$, and $\bar{q}_T = 1.2$.

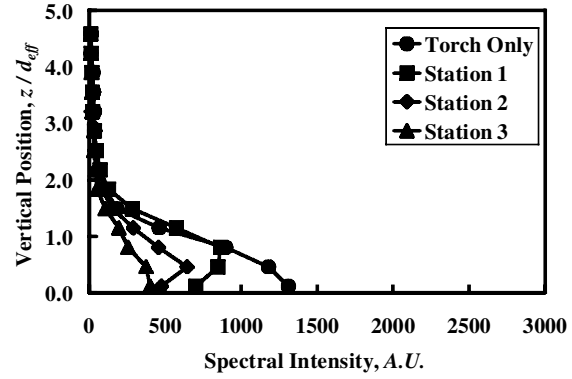

Fig. 19 C_2^* line spectra at 516.5 nm as a function of plasma-torch station with a methane feedstock and ethylene fuel, 2000 W, $\bar{q}_j = 1.5$, and $\bar{q}_T = 1.2$.

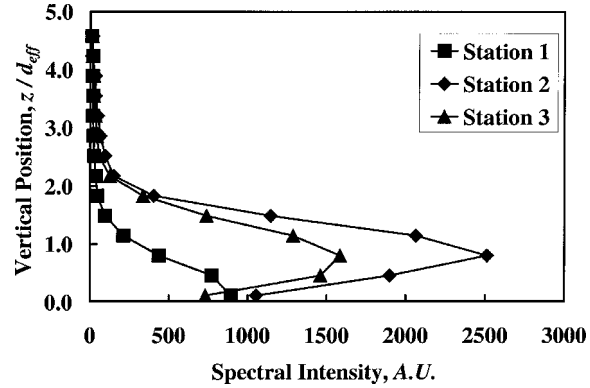

Fig. 20 C_2^* line spectra at 516.5 nm as a function of plasma-torch station with a nitrogen feedstock and ethylene fuel, 2000 W, $\bar{q}_j = 1.5$, and $\bar{q}_T = 1.2$.

20 show the $C_2(0, 0)$ line at 516.5 nm. From the data in the graph in Fig. 19 with the methane torch feedstock, it is seen that the intensity of the C_2^* line with ethylene fuel from the injector and the plasma torch is lower than its intensity from the torch alone. In addition, as the torch is moved farther downstream from the fuel-injector array, the C_2^* concentration falls off, and the penetration of the emission into the main fuel plume is diminished. This could mean that the C_2^* near the surface is actually from the methane plasma rather than from the ethylene fuel; however, further experiments would be necessary to prove this. The experiments with the nitrogen feedstock showed results that are more favorable compared to the methane feedstock in terms of C_2^* levels. Because the levels produced by the nitrogen feedstock are higher and because all of the C_2^* radicals must come from the interaction of the torch plasma with fuel plume, the

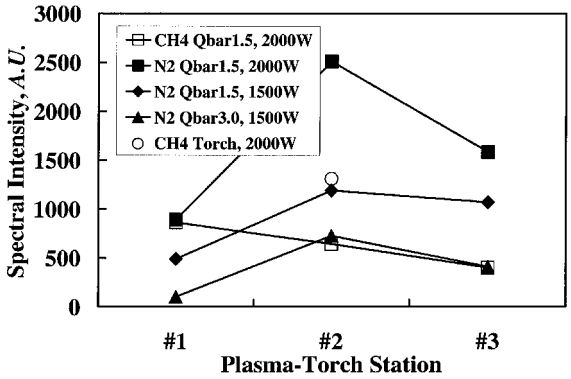

Fig. 21 Trends of the C_2^* line profiles maximum intensity at 516.5 nm as a function of plasma-torch station; methane and nitrogen feedstocks with ethylene fuel.

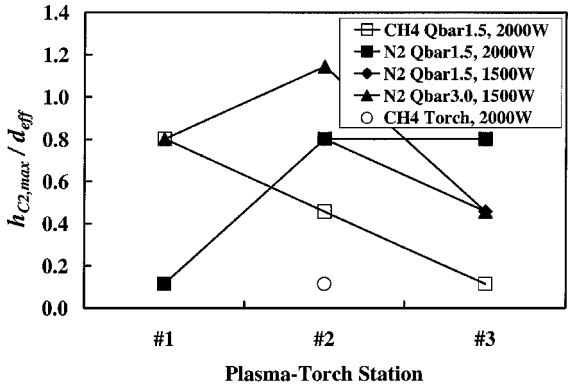

Fig. 22 Penetration height of the C_2^* line profiles maximum intensity at 516.5 nm as a function of plasma-torch station; methane and nitrogen feedstocks with ethylene fuel.

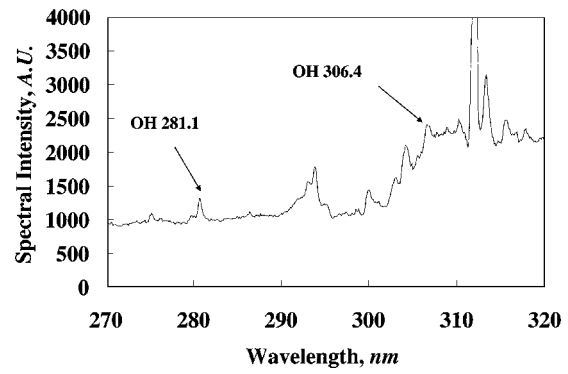

Fig. 23 Spectrogram with long duration exposure shows excited hydroxyl peaks are very weak.

only source of carbon is from ethylene. This indicates a higher level of excited species propagation in the fuel-torch emission plume. It could also be interpreted as indicating a higher amount of heat release, which would be required to increase the amount of excited species in the plume. This is illustrated by the increase in C_2^* line intensity and penetration height of the excited species in Figs. 21 and 22, respectively.

In addition, there is also evidence of a small concentration of excited hydroxyl radicals in the emission plume as identified by the peaks in Fig. 23. Figure 23 was generated with the fiber optic spectrometer with its viewing area focused with a collimating lens to a diameter of about 2.0 mm. The spectrometer was focused on a region 1 cm downstream of the plasma torch and 4.5 mm off above the surface with a 1-s integration time. This location corresponds to a normalized vertical distance of 1.03 d_{eff}. The data shown in Fig. 23 were for an injector momentum-flux ratio of 1.5, with a nitrogen feedstock through the torch at 2000 W. In the graph, excited hydroxyl peaks are shown at 281.1 and 306.4 nm. The 306.4-nm peak is also masked by several other peaks near its wavelength involving excited nitrogen species, which makes it hard to see. Because the emission from OH^* is several orders of magnitude lower than the dominant chemiluminescence, which is evident by inspection of Fig. 14, this shows us that there is little heat release from the combustion of the main fuel. This, compounded with the relatively low amount of CH^* present (another good indicator of heat release) shows us that the predominant portion of the fuel has failed to ignite. As to why little ignition occurred, the main reasons tend to point toward the lack of oxygen in the plume of the injector array compounded with quenching effects from the low temperature of the freestream and fuel.

Conclusions

Cold flow, Mach 2.4 experiments were performed for an initial evaluation of an integrated fuel injection and ignition/flame-holding system consisting of an aerodynamic ramp-injector array with ethylene as the injectant and a plasma torch with various feedstocks. The plasma torch was placed at three downstream locations relative to the injector array.

When interpreting the results from this paper it must be kept in mind that the general flowfield studied was extremely cold (131 K freestream temperature and room temperature ethylene fuel) and that the plasma torch was placed into a fuel-rich region. The three downstream torch locations were set at a close position to the fuel array in an attempt to capitalize on the relatively strong plume vortices near the injector. The initial idea was to wrap the plasma jet up into the plume and away from the surface, allowing the "potential" flame produced to propagate around the fuel plume in its mixing layer. Although this final anticipated effect can not be directly studied in a cold-flow environment, it was thought that, by studying the size and general position of the plume, favorable conditions could be established that may lead to success in a high-temperature scramjet combustor.

It was found that the flame size was very dependent on the plasma-torch feedstock selected. For a given condition (fuel flow rate and torch power), the greatest increase in the size of the flame was due to the local equivalence ratio change at the plasma/fuel plume interface, that is, as the feedstock changed from methane to a nitrogen/hydrogen mixture, to pure nitrogen, and again to air, the flame size significantly increased. This finding suggests that the integrated device should work better the lower the injector jet-to-freestream momentum-flux ratio goes because, as the mass flow from the injector array decreases, the effective distance from the fuel array to the torch increases, and the local equivalence ratio at the torch goes down. Because of this effect, one may also conclude that while operating the torch with a fuel-type feedstock, one may have better success by placing the plasma jet in front of the array, or decoupling it from the fuel arrays line of axial symmetry.

Also note that the chemiluminescence (emission) plume reaction zone is not necessarily the path of the plasma jet feedstock. This was made evident by inspecting the differences in shape of the emission from the operation of the torch with the methane and nitrogen feedstocks behind the fuel injector array. The methane feedstock produced the highest amount of emission near the surface, whereas the nitrogen feedstock emission plume was more prone to penetrate up off the surface of the test section. Hence, the emission seen was really the path of the reaction as altered by the local change in equivalence ratio due to the plasma-torch feedstock.

By inspection of the downstream total temperature results, one can also conclude that the plasma torch plume is, at all torch stations, being lifted up by the counter-rotating vortex motion of the fuel injector's plume. Results show that the core of the temperature plume was 2.5 and 3.5 times higher with the injector in operation at jet-to-freestream momentum-flux ratios of 1.5 and 3.0, respectively, when compared to the height of the torch in operation alone.

When the plasma torch is operated with a methane feedstock, more exited C_2^* radicals are produced, which penetrate farther into

the main ethylene-fuel jet plume with the torch at the closest station (#1) to the injector in the cases studied. In addition, this configuration also had the highest intensity level of all of the excited species measured with the spectrometer (C^*, H^*, CN^*, N_2^*, and CH^*) for the three stations tested. Nitrogen, when compared to methane, produced more C_2^* radicals, indicating more plasma/fuel interactions. These excited species penetrated farther into the main fuel plume and created a larger temperature rise associated with a higher level of heat release in the main fuel plume. Nitrogen also produced higher intensities of CH^*, N_2^*, CN^*, and C_2^* than methane, although methane did produce higher levels of C^* and H^*. The torch at the middle-station (#2) produced the highest level of excited species as measured with the spectrometer at the measurement station 1 cm downstream of the torch orifice. Furthermore, the emission-plume photographs show that, in this case, the excited species penetrated farthest into the main fuel plume and had the longest length.

The emission from OH^* was several orders of magnitude lower than the dominant chemiluminescence produced by the emission plume. This shows us that there is little heat release from the combustion of the main fuel. This, compounded with the relatively low amount of CH^* present (another good indicator of heat release) shows us that the predominant portion of the fuel has failed to ignite. As to why little ignition occurred, the main reasons tend to point toward the lack of oxygen in the plume of the injector array compounded with quenching effects from the low temperature of the freestream and fuel.

Tests of this injector/igniter arrangement in a model scramjet combustor with hot flow are planned. This will permit a full and fair evaluation of the performance of this device.

Acknowledgments

The plasma igniter/aeroramp integration was initially developed under subcontract to and in cooperation with Phoenix Solutions Company under a U.S. Air Force Small Business Innovative Research Phase II plasma igniter program with U.S. Air Force Research Laboratory.

References

[1]Heiser, W. H., Pratt, D. T., Daley, D. H., and Mehta, U. B., "Hypersonic Airbreathing Propulsion," edited by J. S. Przemieniecki, AIAA Education Series, AIAA, Washington, DC, 1994, pp. 305–312.

[2]Hartfield, R. J., Hollo, S. D., and McDaniel, J. C., "Experimental Investigations of a Supersonic Swept Ramp Injector Using Laser Induced Iodine Fluorescence," *Journal of Propulsion and Power*, Vol. 10 No. 1, 1994, pp. 129–135.

[3]Riggins, D. W., and Vitt, P. H., "Vortex Generation and Mixing in Three-Dimensional Supersonic Combustors," *Journal of Propulsion and Power*, Vol. 11, No. 3, 1995, pp. 419–426.

[4]Lewis, D. P., and Schetz, J. A., "Tangential Injection from Overlaid Slots into a Supersonic Stream," *Journal of Propulsion and Power*, Vol. 13, No. 1, 1997, pp. 59–63.

[5]Schetz, J. A., Billig, F. S., Favin, S., and Gilreath, H. E., "Effects of Pressure Mismatch on Slot Injection in a Supersonic Flow," *International Journal of Turbo and Jet Engines*, Vol. 9, No. 2, 1992, pp. 135–146.

[6]Tomioka, S., Jacobsen, L. S., and Schetz, J. A., "Sonic Injection from Diamond-Shaped Orifices into a Supersonic Crossflow," *Journal of Propulsion and Power*, Vol. 19, No. 1, 2003, pp. 104–114.

[7]Schetz, J. A., "Interaction Shock Shape for Transverse Injection," *Journal of Spacecraft and Rockets*, Vol. 7, No. 2, 1970, pp. 143–149.

[8]Fuller, E. J., Mays, R. B., Thomas, R. H., and Schetz, J. A., "Mixing Studies of Helium at High Supersonic Speeds," *AIAA Journal*, Vol. 30, No. 9, 1992, pp. 2234–2243.

[9]Barber, M. J., Roe, L. A., and Schetz, J. A., "Normal, Sonic Helium Injection Through a Wedge-Shaped Orifice in Supersonic Flow," *Journal of Propulsion and Power*, Vol. 13, No. 2, 1997, pp. 257–263.

[10]McClinton, C. R., "The Effect of Injection Angle on the Interaction Between Sonic Secondary Jets and a Supersonic Freestream," NASA TND-6669, Feb. 1972.

[11]Rogers, R. C., "A Study of the Mixing of Hydrogen Injected Normal to a Supersonic Airstream," NASA TN L-7386, March 1971.

[12]Jacobsen, L. J., Schetz, J. A., Gallimore, S. D., and O'Brien, W. F., "Mixing Enhancement by Jet Swirl in a Multiport Injector Array in Supersonic Flow," *Proceedings of the 3rd ASME/ISME Joint Fluids Engineering Conference*, FEDSM99-7248, July, 1999.

[13]Kraus, D. K., and Cutler, A. D., "Mixing of Swirling Jets in a Supersonic Duct Flow," *Journal of Propulsion and Power*, Vol. 12, No. 1, 1996, pp. 170–177.

[14]Cutler, A. D., and Johnson, C. H., "The Use of Swirling Jet Pairs to Provide Rapid Fuel Penetration in Scramjet Combustors," AIAA Paper 95-0099, Jan. 1995.

[15]Schetz, J. A., *Injection and Mixing in a Turbulent Flow*, AIAA, New York, Chap. V, 1980, pp. 111–122.

[16]Povinelli, L. A., and Ehlers, R. C., "Swirling Base Injection for Supersonic Combustion Ramjets," *AIAA Journal*, Vol. 10, No. 9, 1972 pp. 1243–1244.

[17]Schetz, J. A., and Swanson R. C., "Turbulent Jet Mixing at High Supersonic Speeds," *Zeitschrift Für Flugwissenschaften*, Vol. 21, No. 5, 1973, pp. 166–173.

[18]Schetz, J. A., Thomas, R. H., and Billig, F. S., "Mixing of Transverse Jets and Wall Jets in Supersonic Flow," *Separated Flows and Jets*, edited by V. V. Koslov and A. V. Dovgal, Springer-Verlag, Berlin, 1991, pp. 807–837.

[19]Cox, S. K., Fuller, R. P., and Schetz, J. A., "Vortical Interactions Generated by a Injector Array to Enhance Mixing in a Supersonic Flow," AIAA Paper 94-0708, Jan. 1994.

[20]Cox-Stouffer, S. K., and Gruber, M. R., "Effects of Spanwise Injector Spacing on Mixing Characteristics of Aerodynamic Ramp Injectors," AIAA Paper 98-3272, July 1998.

[21]Fuller, R. P., Wu, P.-K., Nejad, A. S., and Schetz, J. A., "Comparison of Physical and Aerodynamic Ramps as Fuel Injectors in Supersonic Flow," *Journal of Propulsion and Power*, Vol. 14, No. 2, 1998, pp. 135–145.

[22]Schetz, J. A., Cox-Stouffer, S. K., and Fuller, R. P., "Integrated CFD and Experimental Studies of Complex Injectors In Supersonic Flows (Invited)," AIAA Paper 98-2780, June 1998.

[23]Jacobsen, L. J., Schetz, J. A., and Ng, W. F., "The Flowfield Near a Multiport Injector Array in a Supersonic Flow," *Journal of Propulsion and Power*, Vol. 16, No. 2, 2000, pp. 216–226.

[24]Eklund, D. R., and Gruber, M. R., "Study of a Supersonic Combustor Employing an Aerodynamic Ramp Pilot Injector," AIAA Paper 99-2249, June 1999.

[25]Gruber, M., Donbar, J., Jackson, T., Mathur, T., Eklund, D., and Billig, F., "Performance of an Aerodynamic Ramp Fuel Injector in a Scramjet Combustor," AIAA Paper 2000-3708, July 2000.

[26]Jacobsen, L. J., Gallimore, S. D., Schetz, J. A., and O'Brien, W. F., "An Improved Aerodynamic Ramp Injector in Supersonic Flow," AIAA Paper 2001-0518, Jan. 2001.

[27]Weinberg, F. J., "Advanced Combustion Methods," edited by F. J. Weinberg, Academic Press, Inc., London, Chap. V, 1986, pp. 277–330.

[28]Stouffer, S., O'Brien, W., and Roby, R., "Improved Plasma Torch for Ignition and Flame Holding in Supersonic Combustion," AIAA Paper 89-2945, July 1989.

[29]Kim, J., Clemens, N., and Varghese, P., "Experimental Study of an Underexpanded Pulsed Plasma Jet," AIAA Paper 99-0452, Jan. 1999.

[30]Kimura, I., Aoki, H., and Kato, M., "The Use of a Plasma Jet for Flame Stabilization and Promotion of Combustion in Supersonic Air Flows," *Combustion and Flame*, Vol. 42, 1981, pp. 297–305.

[31]Takita, K., Masuya, G., Sato, T., and Ju, Y., "Effects of Addition of Radicals on Burning Velocity," *AIAA Journal*, Vol. 39, No. 4, 2001, pp. 742–744.

[32]Takita, K., Takatori, F., and Masuya, G., "Effect of Plasma Torch Feedstock on Ignition Charecteristics in Supersonic Flow," AIAA Paper 2000-3586, July 2000.

[33]Takita, K., Uemoto, T., Sato, T., Ju, Y., Masuya, G., and Ohwaki, K., "Ignition Charecteristics of Plasma Torch for Hydrogen Jet in an Airstream," *Journal of Propusion and Power*, Vol. 16, No. 2, 2000, pp. 227–233.

[34]Masuya, G., Takita, K., Sato, T., Ohwaki, K., Takahashi, K., Uemoto, T., Ju, Y., and Matsumoto, M., "Ignition of Parallel and Low Angle Hydrogen Jet by Plasma Torch," 14th International Symposium on Air Breathing Engines Conf., ISABE Paper 99-7051, Sept. 1999.

[35]Wagner, T., O'Brien, W., Northam, G., and Eggers, J., "Plasma Torch Igniter for Scramjets," *Journal of Propulsion and Power*, Vol. 5, No. 5, 1989, pp. 548–554.

[36]Northam, G., McClinton, C., Wagner, T., and O'Brien, W., "Development and Evaluation of a Plasma Jet Flameholder for Scramjets," AIAA Paper 84-1408, June 1984.

[37]Sato, Y., Sayama, M., Ohwaki, K., Masuya, G., Komuro, T., Kudou, K., Murakami, A., Tani, K., Wakamatsu, Y., Kanda, T., Chinzei, N., and Kimura, I., "Effectiveness of Plasma Torches for Ignition and Flameholding in Scramjet," *Journal of Propulsion and Power*, Vol. 8, No. 4, 1992, pp. 883–889.

[38]Warris, A., and Weinberg, F., "Ignition and Flame Stabilization by Plasma Jets in Fast Gas Streams," *Twentieth Symposium (International) on Combustion*, Combustion Inst., Pittsburgh, PA, 1984, pp. 1825–1831.

[39]Shuzenji, K., Kato, R., and Tachibana, T., "Ignition Characteristics of Arc Discharges Exposed to Supersonic Airflows," AIAA Paper 2000-0617, Jan. 2000.

[40]Fuji, S., Shuzenji, K., Kato, R., and Tachibana, T., "Augmentation of Ignition Arcs for Air Breathing Combustion by Teflon Sublimates," AIAA Paper 1998-3215, July 1998.

[41]Kanda, T., Hiraiwa, T., Mitani, T., Tomioka, S., and Chinzei, N., "Mach 6 Texting of a Scramjet Engine Model," *Journal of Propulsion and Power*, Vol. 13, No. 4, 1997, pp. 543–551.

[42]Gallimore, S. D., Jacobsen, L. S., O'Brien, W. F., and Schetz, J. A., "An Integrated Aeroramp Injector/Plasma Igniter for Hydrocarbon Fuels in a Supersonic Flow, Part 2: Experimental Studies of the Operating Conditions," AIAA Paper 2001-1767, April 2001.

[43]Pearse, R. W. B., and Gaydon, A. G., *The Identification of Molecular Spectra*, Wiley, New York, 1963, pp. 94, 95, 112, 113, 211.